

CARBON NANOMATERIALS FOR CHEMICAL AND BIOLOGICAL SENSING

by

Ian Matthew Feigel

B.S., Erskine College, 2009

Submitted to the Graduate Faculty of
The Kenneth P. Dietrich School of Arts and Sciences in partial fulfillment
of the requirements for the degree of
Master of Science

University of Pittsburgh

2012

UNIVERSITY OF PITTSBURGH
KENNETH P. DIETRICH SCHOOL OF ARTS AND SCIENCES

This thesis was presented

by

Ian Matthew Feigel

It was defended on

December 9, 2011

and approved by

Dr. Adrian C. Michael, Professor, Department of Chemistry

Dr. Geoffrey R. Hutchison, Assistant Professor, Department of Chemistry

Committee Chair: Dr. Alexander Star, Associate Professor, Department of Chemistry

Copyright © by Ian Matthew Feigel

2012

CARBON NANOMATERIALS FOR CHEMICAL AND BIOLOGICAL SENSING

Ian Matthew Feigel, M.S.

University of Pittsburgh, 2012

Carbon nanotubes (CNTs), first discovered in 1991, are cylindrical structures composed of atomically thin sp^2 hybridized carbon which can be visualized as a rolled up sheet of graphene. CNTs have excellent mechanical and electronic properties which make them a very promising new material. Typically, CNTs have diameter between one and several nanometers, comparable to the size of individual molecules, and lengths that can exceed several micrometers, which enables integration into microscale electronics. Most interestingly, CNTs electronic properties are very sensitive to changes in their local chemical environment, as all carbon atoms are located on the surface. By placing CNTs between two electrodes, they can function as a resistor or transistor for sensor applications, and through addition functionalization, the CNTs can serve as ultrasensitive, selective devices.

Herein, we report the specific functionalization of single-walled carbon nanotubes (SWNTs) for chemical and biological sensing. First, SWNTs have been decorated with metal oxide nanoparticles and a hydrophilic polymer for the detection of CO_2 gas. The interactions of the SWNTs with the functional layers have been characterized in detail. Secondly, oxidized SWNTs functionalized with a pH sensitive polymer have been developed for selective detection of the pH of buffered solutions, with the ability to distinguish between 0.1 pH units. This device was also further functionalized to demonstrate detection of CO_2 and H_2 gas.

TABLE OF CONTENTS

1.0	INTRODUCTION.....	1
1.1	PHYSICAL AND ELECTRONIC STRUCTURE OF CNTS	1
1.2	INTEGRATION OF SWNTS INTO ELECTRONIC DEVICES	3
1.3	SWNT-BASED ELECTRONIC DEVICES	6
2.0	RESEARCH PROGRESS.....	10
2.1	CO₂ DETECTION.....	10
	2.1.1 Experimental Details	12
	2.1.2 Results and Discussion	13
	2.1.3 Prototype Development.....	21
2.2	pH SENSING	23
	2.2.1 Experimental Details	25
	2.2.2 Results and Discussion	27
3.0	FUTURE ENDEAVORS (TOWARDS BIOSENSING).....	36
	BIBLIOGRAPHY.....	38

LIST OF FIGURES

Figure 1 Carbon Nanotube (CNT) Structure.	4
Figure 2 Band diagram depicting the formation of a Schottky Barrier (SB) between a semiconducting SWNT and a metal.	5
Figure 3 SWNT based chemiresistor.	7
Figure 4 SWNT based field-effect transistor (FET).	9
Figure 5 CO ₂ detection based on nanoparticle/polymer modified SWNTs.	14
Figure 6 CO ₂ detection based on different polymer functionalized SWNTs.	15
Figure 7 CO ₂ detection mechanism experiments.	19
Figure 8 Prototype development.	22
Figure 9 pH sensor material characterization.	29
Figure 10 Electrical measurements of PAA/o-SWNT.	30
Figure 11 Field-effect transistor characterization of PAA/o-SWNT.	32
Figure 12 Further functionalization of PAA/o-SWNT for detection of other analytes.	34
Figure 13 Proposed scheme for biosensor development.	37

1.0 INTRODUCTION

Carbon nanotubes (CNTs) have drawn very much attention over the last two decades due to their many exciting applications. CNTs, a member of the fullerene family,¹ are cylindrical structures composed of carbon atoms. Typically, carbon nanotubes are one to several nanometers in diameter and can be up to several micrometers in length. The high aspect ratio and nanoscale diameter of CNTs create unique properties that allow for exciting applications. For instance, their long length allows for facile integration in current micrometer sized electronics, while their nanoscale diameter allows them to probe molecular systems by directly plugging into individual or assemblies of molecules. Additionally, single-walled carbon nanotubes (SWNTs) have all carbon atoms on the surface and therefore are very sensitive to their local chemical environment, making SWNTs ideal for chemical and biological sensing. By placing SWNTs between two metal electrodes they can function as a sensitive resistor or transistor for sensor applications. These properties and more make SWNTs an ideal platform for studying chemical and biological systems.

1.1 PHYSICAL AND ELECTRONIC STRUCTURE OF CNTS

Although existence of carbon nanotubes was first reported in the 1950s,² their electronic structure was not described in details until ground breaking work by Sumio Iijima in 1991.³

Carbon nanotubes can best be visualized as a rolled up sheet of atomically thin sp^2 hybridized carbon, as depicted in Figure 1A. When only a single cylinder is present, CNTs are deemed single-walled (SWNT) and when the tubes consist of many concentrically nested tubes, they are referred to as multi-walled (MWNT). Schematic representations of both of these tubes is shown in Figure 1B, with the innermost red CNT representing the SWNT.

Another important physical property of CNTs is their inherent chirality. Conceptually, this can be described as the way in which the CNT is rolled up from a graphene sheet. For example, it can be imagined that a square graphene sheet can be rolled up in a way in which the two opposite ends meet or where the two opposite corners overlap. This geometry of SWNTs is described by two vectors, referred to as roll up vectors, which are denoted as (n,m) .^{4, 5} A schematic representation of these vectors is presented in Figure 1C. As each carbon atom in a graphene sheet has three sp^2 electrons within the plane and one p orbital that projects orthogonally from the surface, a delocalized π -electron structure is present.⁶ The roll up vectors help to represent the overlapping of these orbitals. Such overlap indicates whether a SWNT is metallic or semiconducting. Specifically, metallic CNTs have $n-m$ values equal to $3k$, where k is any integer including zero. All other values of $n-m$ will represent semiconducting SWNTs.

Looking at the electronic structure of CNTs, the valence and conduction bands can be considered the CNTs highest occupied molecular orbital, HOMO, and the lowest unoccupied molecular orbital, LUMO, respectively. Metallic CNTs have a finite density of allowed electronic states at their Fermi level, the position between the HOMO and LUMO, whereas semiconducting CNTs, have a region of forbidden electronics states, i.e. a band gap. Several names have been assigned to classes of CNTs with particular roll up vectors and are illustrated in Figure 1C. For instance zigzag CNTs have a roll up vector of $(n,0)$, armchair CNTs have $n=m$,

and chiral CNTs have $n \neq m$. It is important to note that current synthetic techniques results in mixtures of CNTs; approximately one-third are metallic and two-thirds semiconducting.⁷

1.2 INTEGRATION OF SWNTS INTO ELECTRONIC DEVICES

The relatively long length of SWNT (microns) allows for facile integration into electronic devices in order to serve as conducting channels of electronic devices. When placing semiconducting SWNTs in between two metallic electrodes, a unique phenomenon occurs. Due to mismatches in the work functions of the metal electrode and the semiconductor, the Fermi levels of the two materials will equilibrate, which in turn bends the p-type semiconductor valence band toward higher energies.⁸ In ambient conditions, the valence band of semiconducting SWNTs is partially depleted of electron density, thus making them p-type semiconductors. P-type semiconductors conduct holes instead of electrons. When this SWNT comes into contact with a metal, some electron density is donated from the metal to the valence band of the SWNT, pushing it to a higher energy. There is a region at the SWNT-metal interface where increased electron density forms in the SWNT valence band. This region is referred to as a depletion region, which forms a potential barrier, termed Schottky Barrier (SB). The SB inhibits the transfer of holes from the metal into the SWNT valence band. A representation of a SB at the metal-semiconducting SWNT interface is shown in Figure 2.

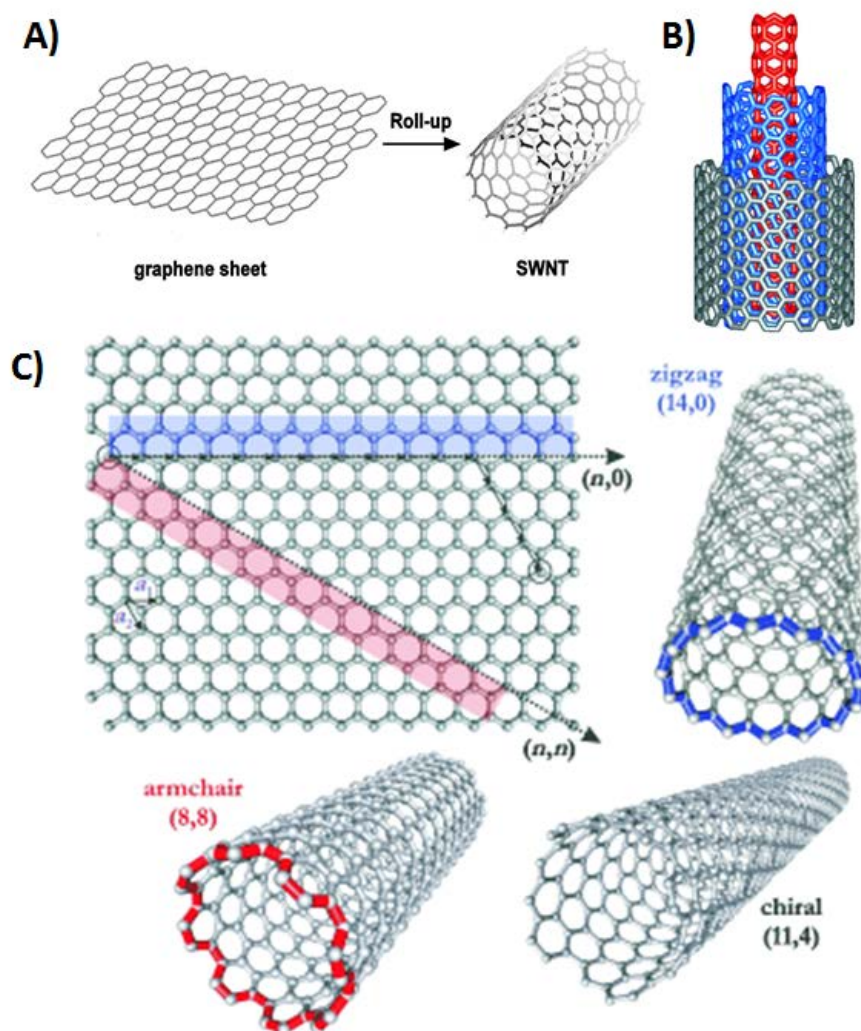


Figure 1 Carbon Nanotube (CNT) Structure. A) Representation of carbon nanotube (CNT) formation by rolling up a sheet of graphene. Adapted with permission from reference 4. Copyright 2000 American Chemical Society. B) Illustration of a multi-walled carbon nanotube (MWNT) composed of concentric walls. The innermost red CNT is considered a single-walled carbon nanotube (SWNT). C) Schematic representation of a graphene sheet specifically showing the roll up vectors (n,m) . Resulting CNTs from various rollup vectors are depicted. Adapted with permission from reference 5. Copyright 2005 Wiley-VCH Verlag GmbH & Co. KGaA.

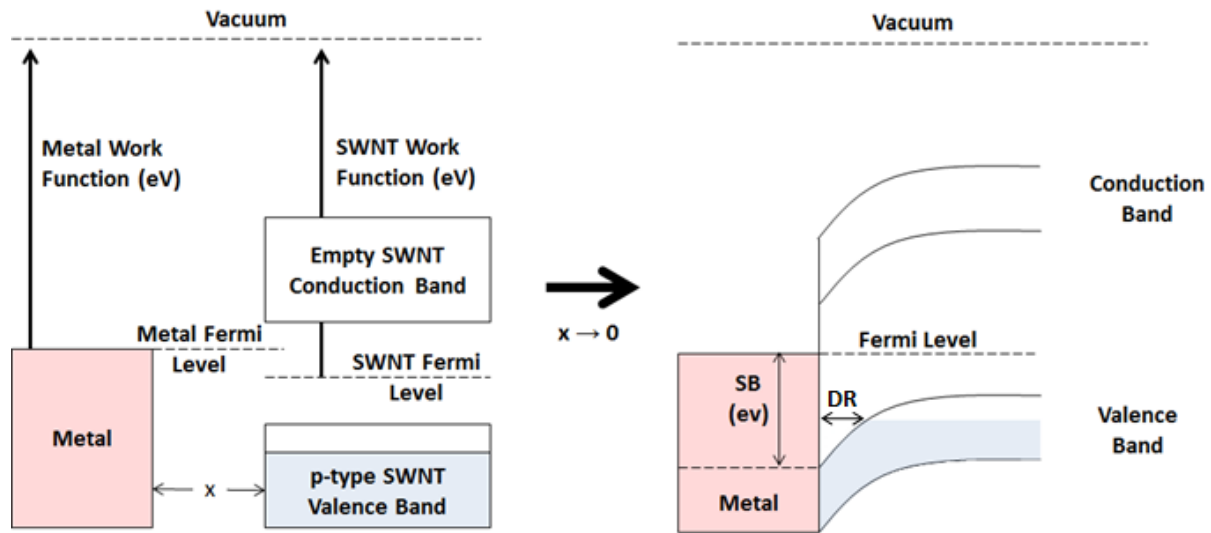


Figure 2 Band diagram depicting the formation of a Schottky Barrier (SB) between a semiconducting SWNT and a metal. When separated by some macroscopic distance, x , the metal and p-type semiconducting SWNTs have different work functions and Fermi levels. Upon contact, Fermi level equilibration occurs, which results in donation of electron density from the metal electrode into the SWNT valence band. This results in an upward bending of the valence band creating a depletion region (DR) at the interface which may extend several nanometers into the SWNT. This region of increased electron density produces a potential barrier for movement of holes between the SWNT valence band and the metal, known as Schottky Barrier.

1.3 SWNT-BASED ELECTRONIC DEVICES

The two most commonly used SWNT based electronic devices, resistors and transistors, both utilize SWNTs as the conductive channel between two metal electrodes. Gold (Au) is typically used for devices, yet palladium (Pd) has been found to make excellent electrical connections with SWNTs.⁹ It is believed that a close match of work functions of the metal (Au ~ 5.0, Pd ~ 5.1 eV) and the SWNT (~5 eV) should result in small SBs.¹⁰⁻¹² Of the two types of electronic devices, the simpler design consists of either a single or network of SWNTs incorporated between two metal electrodes on an insulating substrate. This configuration, termed chemiresistor, is based on the SWNT acting as a chemically sensitive resistor. A constant bias voltage is applied through the nanotube (network), and the resistance (R; ohms) or conductance (G; Siemens) is measured as a function of both time and analyte concentration. Any interaction of the analyte with the SWNT which modifies the electron density in the valence band will result in changes in the device conductance and can be easily measured. For example, if a molecule donates electrons into the valence band of the SWNT, the concentration of charge carriers (holes) will be diminished resulting in a decrease in SWNT conductance. However, molecular adsorption can introduce charge scattering sites along the SWNT and molecular interactions with the metal electrode can modify the device SB both resulting in changes in device characteristics, ultimately complicating the understanding of such devices. An example of an SWNT chemiresistor device is shown in Figure 3A.¹³ Here the schematic describes a chemiresistor device composed of a network of SWNTs deposited on top of gold electrodes, labeled source (S) and drain (D), previously deposited on an insulating SiO₂ surface. A bias voltage (V_{SD}) of 50 mV is applied through the nanotube network via the source and drain electrodes and the conductance is plotted in real time (Figure 3B). It is important to note that a

single nanotube could be used in the place of the network, however is not advantageous. Higher conductance ranges are allowed by using networks of SWNTs in addition to being more defect tolerant as there are multiple conduction channels. Typical experiments involve monitoring of the conductance of the nanotube network in real time as a function of the analyte in question.

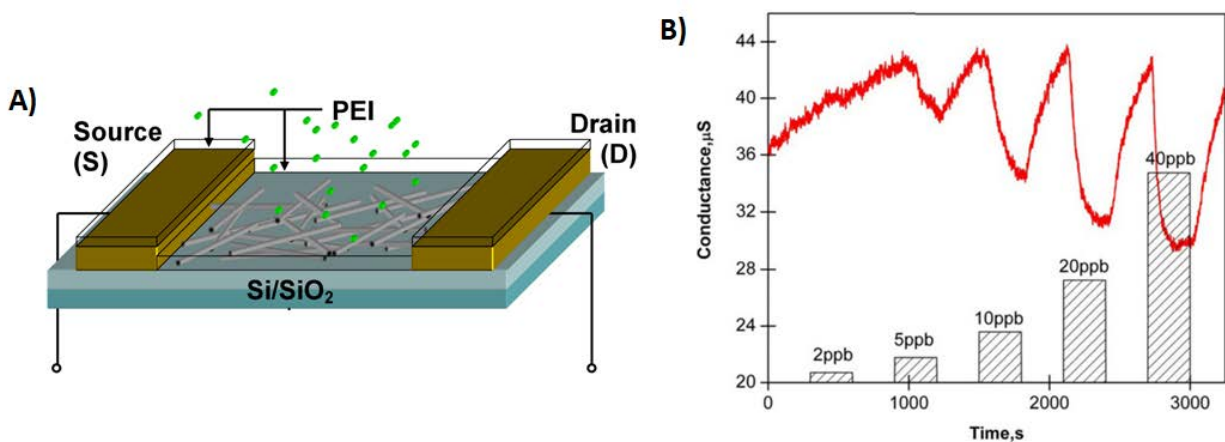


Figure 3 SWNT based chemiresistor. A) Schematic diagram of a carbon nanotube chemiresistor microsensor. Interdigitated gold electrodes are deposited onto a Si/SiO₂ substrate via electron beam evaporation, followed by deposition of SWNTs and the chemical analyte-specific functionalization layer. A constant source drain voltage is applied and the resulting conductance of the SWNT network is measured. B) Typical device response monitoring the conductance of the SWNT network in real time as a function of the analyte, in this case nitric oxide gas. Adapted with permission from reference 13.

The second device design, termed carbon nanotube field-effect transistor (CNTFET), was first reported in 1998.^{14, 15} The main difference between this design and the chemiresistor is the presence of a back gate in which a gate voltage (V_G) can be applied to modulate the electrical conductance through the source and drain. Typically, the device conductance is monitored as a function of gate voltage and the device output is called a transistor transfer characteristic. The behavior of such devices depends on the formation of SBs at the SWNT-metal contact interface.¹⁶ Sweeping the gate voltage to more negative values will decrease the barrier for hole transmission and therefore increase the device conductance, and *vice versa*.¹⁷ A schematic representation of the circuit diagram is shown in Figure 4A.¹⁸ An AFM image of a single nanotube device shown in Figure 4B, and a scanning electron microscopy (SEM) image of a network device is shown in Figure 4C. A representative transistor transfer characteristics curve is shown in Figure 4D. Certain chemical species can cause changes to this characteristic. For instance, electron donating molecules will shift this curve toward more negative gate voltages and result in a decreased conductance over the whole range of gate voltages. Donation of electrons into the valence band of the SWNT will result in charge carrier recombination, therefore decreasing the number of current carrying holes. Additionally, the increased electron density increases the SB and therefore decreases the transmission of holes. Understandably, electron withdrawing molecules have the opposite effect.

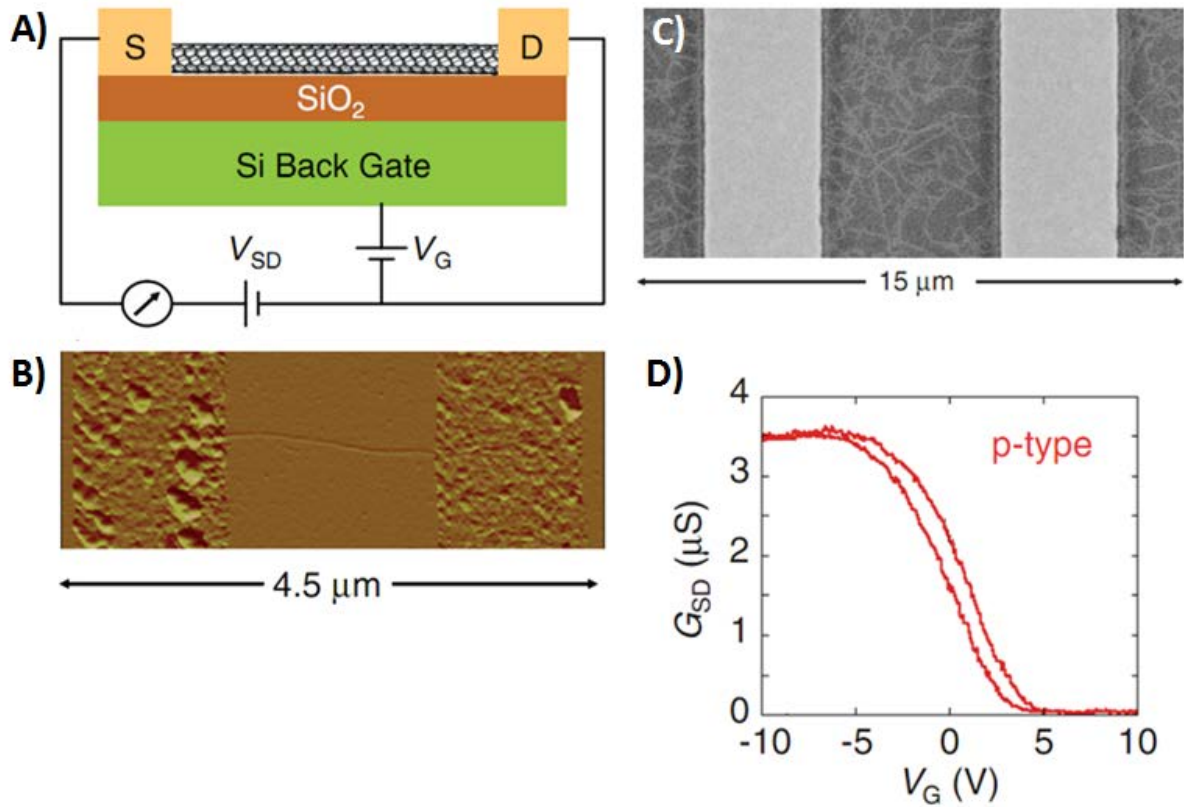


Figure 4 SWNT based field-effect transistor (FET). A) Schematic of a carbon nanotube field-effect transistor (CNTFET) with a semiconducting SWNT connecting two Au electrodes, labeled source and drain. B) AFM image of a single nanotube device. C) Scanning electron microscopy image of a CNTFET device using a network of CNTs. D) Typical CNTFET transfer characteristics; source-drain conductance as a function of applied gate. Adapted with permission from reference 18. Copyright 2007 Wiley-VCH Verlag GmbH & Co. KGaA.

2.0 RESEARCH PROGRESS

Published Work to Date:

“Biosensors based on One-Dimensional Nanostructures” I. M. Feigel, H. Vedala, A. Star, *J. Mater. Chem.*, 2011, **21**, 8940-8954.

Manuscripts in Preparation:

- 1) CO₂ detection manuscript : I. Feigel, B. L. Allen, A. Star
- 2) pH sensor manuscript: I. M. Feigel, P. Gou, A. Star

2.1 CO₂ DETECTION

Carbon dioxide (CO₂) gas plays crucial roles in medical,¹⁹ industrial,²⁰ and environmental settings²¹. For instance, of physiological relevance, respiratory failure can occur instantly or over the course of time, making accurate predictions nearly impossible. For this reason, it has

been proposed that continuous monitoring of respiratory activity be performed using low-cost, miniature CO₂ sensors capable of real-time detection.²² Likewise, real-time monitoring of CO₂ gas has been suggested for industrial and environmental applications. CO₂ emissions pose a rising concern because of their overall contribution to global warming. Thus, continual monitoring is necessitated in order to evaluate current emissions levels. Numerous technologies have been implemented to detect CO₂ including solid electrolyte sensors,²³ conductive thick films,²⁴ and fiber-optic luminescence.²⁵ Currently, the most common technology for CO₂ sensing is non-dispersive infrared spectroscopy (NDIR);²⁶ however, its power consumption, size, and cost prohibit incorporation of this technology into wide-spread sensor networks for CO₂ monitoring. To surpass these shortcomings, developments in nanotechnology-based platforms have been proposed for the detection of CO₂ gas. Such methods include surface acoustic wave sensors that rely on a piezoelectric frequency change,²⁷ amperometric electrochemical methods using modified electrodes,²⁸ and capacitive and resistive measurements using carbon nanotubes^{29, 30}. In the last case, chemical vapor deposition (CVD) grown single-walled carbon nanotubes (SWNTs) were used in a solid-state field-effect transistor (FET) and functionalized by poly(ethylene imine) (PEI) polymer. Introduction of CO₂ gas resulted in a change in conductance of the SWNT-FET device, presumably through the formation of carbamates and a subsequent withdrawal of electron density from the n-type devices.³⁰ Of important note, however, SWNT-based FET devices possess a number of impurities such as residual catalyst particles, photoresist, and chemical residues that all may impart sensitivity toward gas detection. In this essence, these factors pose an impediment for understanding the mechanism of gas sensing. Thus, as a means to elucidate the mechanism for detection of CO₂ using this class of

solid-state sensors, a systematic approach has been implemented to examine the function of each component(s).

2.1.1 Experimental Details

Chemicals and Materials: SWNTs were purchased from Carbon Solutions, Inc. (P2-SWNTs). Water-free branched poly(ethylene imine) (PEI) with a typical M_w 25,000 was purchased from Aldrich, St. Louis, MO. γ -Fe₂O₃ nanoparticles and Nafion were purchased from Sigma Aldrich. Certified N₂ (pure) and CO₂ (10% diluted with N₂) were purchased from Valley National Gases, Inc., PA. Mass Flow Controllers MFC (UNIT Instruments, Inc. MKS, Inc.) were controlled by house-built electronics.

Characterization: pH measurements were performed in aqueous by a SG8 – SevenGo pro pH/ion meter (Mettler Toledo) calibrated by buffer solution 7 (phosphates) and buffer solution 4 (biphthalates) from JT Baker. Scanning electron micrograph (SEM) images were taken with a Philips XL-30 FEG microscope. The electron beam accelerating voltage was held constant at 10.0 keV for all samples. Aqueous solutions buffered from pH values of 2 to 12 were prepared based on published methods.^{31,32}

Device Fabrication: SWNTs (0.01 mg) were suspended in 20 mL of dimethylformamide (DMF) through ultrasonication for 5 min. Pre-patterned interdigitated electrodes were fabricated on a Si/SiO₂ substrate (oxide thickness: ~200 nm). Electrodes consisted of a titanium adhesion layer (300 Å) and gold contact layer (1,000 Å). Chips (2 mm x 2 mm) were subsequently diced from a 4" wafer and wedge-bonded with gold wire into a 40-pin ceramic dual in-line package

(CERDIP), followed by passivation of the system with PDMS. Approximately 10 μL of the SWNT suspension was drop-cast on the chip and vacuum baked for 1 hr at 150 $^{\circ}\text{C}$ prior to use. Further functionalization was performed by drop-casting metal oxide nanoparticles (1 mM in acetone) at a volume of 1 μL and drying in ambient. PEI (0.1 wt. % aq) was then drop-cast at a volume of 3 μL .

2.1.2 Results and Discussion

Here we investigate the mechanism of CO_2 detection using SWNTs by reconstructing the sensor architecture using a layer-by-layer approach. Using a clean Si/SiO₂ wafer with pre-fabricated interdigitated Au electrodes and drop-casting individual elements such as commercially available, purified SWNTs, metal oxide nanoparticles, and polymers, the role of each sensor component was analyzed. SWNTs were needed as a transduction pathway for resistive measurements and were utilized throughout these studies. Moreover, as they exhibit minimal sensitivity to CO_2 gas, it can be inferred that additional factors are responsible for viable sensitivity to occur. Initial observations revealed that coating of SWNT devices by poly(ethylene imine) (PEI) polymer alone was not sufficient to elicit a good CO_2 response, suggesting that the presence of residual catalyst in the form of metal oxides may play a more significant role. Conversely, metal oxide nanoparticles without the use of a hydration layer inhibited the detection of CO_2 gas. Such observations lend credibility to a cooperative effect between SWNTs, metal oxide nanoparticles, and the polymer layer. Additionally, substituting the PEI polymer layer with a Nafion layer promoted similar sensitivity towards CO_2 gas, signifying that a polymer layer is needed for hydration of the system, but plays little role beyond this. We propose, based upon these observations, that a localized electrostatic gating effect

around the metal oxide nanoparticle/SWNT interface is responsible for CO₂ sensitivity, where the hydrated polymer layers act to convert CO₂ to carbonic acid.

Figure 5A illustrates the general schematic for solid-state measurements using SWNTs as the transduction pathway. Devices were fabricated as described in the experimental section above. Figure 5B further shows an amplified optical image of the chip in use and a scanning electron micrograph of a device modified with both metal oxide nanoparticles and polymer.

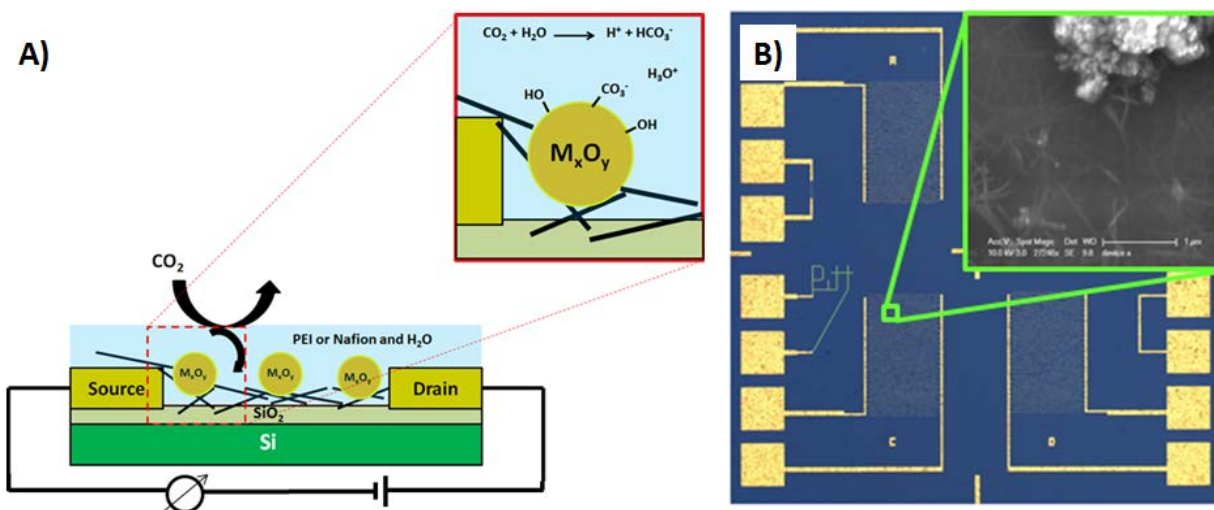


Figure 5 CO₂ detection based on nanoparticle/polymer modified SWNTs. A) Generalized scheme depicting CO₂ detection with a carbon nanotube network modified with metal oxide (M_xO_y) nanoparticles and a polymer layer. CO₂ dissolves into the polymer layer and reacts with ambient water to form carbonic acid. Upon decreases in the pH of the solution bicarbonate displaces OH⁻ groups on the surface of the metal oxide nanoparticles, changing the surface potential and effectively electrostatically gating the SWNT network. B) Optical image of the chip layout. Inset shows a scanning electron microscope (SEM) image of the modified SWNT network functionalized with metal nanoparticles and polymer.

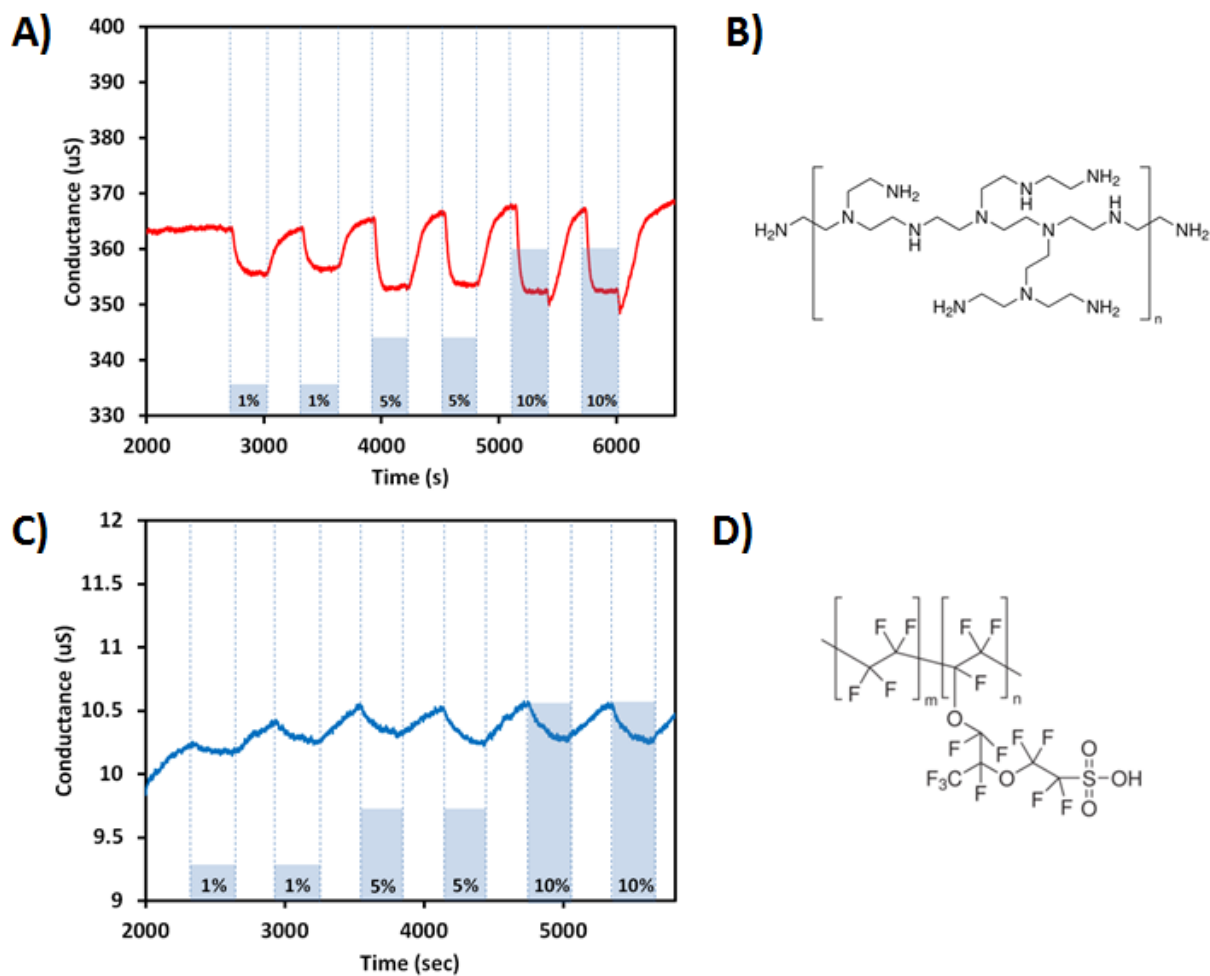


Figure 6 CO_2 detection based on different polymer functionalized SWNTs. A) Conductance vs. time plot of SWNT network, modified with 0.01 wt. % PEI and γ - Fe_2O_3 nanoparticles exposed to 1-10% CO_2 pulses diluted with pure N_2 at 52% RH. B) Structure of PEI. C) Conductance vs. time plot of SWNT network, modified 0.0025 wt. % Nafion and γ - Fe_2O_3 nanoparticles exposed to 1-10% CO_2 pulses (5 min) diluted with pure N_2 at 52% RH. D) Structure of Nafion.

In order to elucidate the function of particular elements within SWNT solid-state devices, we began investigating a system of SWNTs, γ -Fe₂O₃ nanoparticles (Sigma Aldrich), and PEI (aq) polymer (0.1 wt. %). Devices were tested in a four-socket printed circuit board (PCB) connected to a Keithley 708A switching mainframe and Keithley 2602 dual-source meter. A constant voltage of 50 mV was used, and conductance measurements were recorded using Zephyr software.³³ All tested chips were subjected to humidified N₂ (pure) and CO₂ (1-10%) at a total flow rate of 300 sccm (cm³/min) in ambient. A saturated salt solution of sodium bicarbonate (NaHCO₃) was used to provide 52% relative humidity, while preventing further solvation of CO₂ gas.³⁴ Conductance measurements were performed in real-time with set intervals between “on” and “off” states for CO₂ exposure. Figure 6A shows the typical response of a device fabricated by drop-casting Fe₂O₃ nanoparticles (1 mM) and PEI (0.1 wt. %) to 1-10% CO₂ diluted with pure N₂ at 52% relative humidity. As illustrated, at each “on” cycle of CO₂, a decrease in conductance is observed. The conductance then begins to recover to its initial value after CO₂ is removed from the system and replaced with pure N₂. Moreover, the relative response scales with the concentration of CO₂ over the tested regime for multiple devices.

Altering the system slightly, we replaced the PEI polymer layer with a Nafion (0.0025 wt. %) polymer layer through drop-casting 3 μ L on a new device with SWNTs and iron oxide nanoparticles. A comparable response to increasing concentrations of CO₂ is observed, similar to that of PEI (Figure 6C). Of important note, Nafion is a sulfonated tetrafluoroethylene-based fluoropolymer, in contrast to PEI consisting of numerous branched primary, secondary, and tertiary amines. As was previously stated, it has been suggested that carbamate formation is the predominant mechanism for CO₂ detection using SWNT devices modified by PEI.³⁰ However, Nafion cannot follow this proposed scheme as no amines exist for reaction to occur. A more

probable explanation involves the formation of carbonic acid in the hydrated polymer layer, followed by deprotonation into hydronium and bicarbonate ions, thus resulting in an overall pH decrease localized on the SWNT-based device, as will be further explained. Based upon these assumptions, we further examined the role of metal oxide nanoparticles in the detection of varying concentrations of CO₂ gas.

A closer examination into the physical properties of the tested metal oxide nanoparticles reveals a possible electrostatic gating effect with the SWNT-based device, contingent upon the P.Z.C. of the metal oxide nanoparticles. Such potential can be related to pH and the Nernst equation can be written as:³⁵ $[E = (2.303 R_g T [(P.Z.C.) - pH]) / F]$, where R_g is the gas constant, T is temperature, and F is Faraday's constant. At room temperature, this equation can be further simplified to: $[E \approx 0.06 [(P.Z.C.) - pH]]$. It is probable that the change of the initial more negative surface potential and progressive shift toward more positive surface potential of metal oxide nanoparticles in the presence of CO₂ acts as a local electrostatic gate.

These types of interactions between CO₂ and metal oxide interfaces have previously been studied spectroscopically.³⁶ In essence, CO₂ gas combines with water to form carbonic acid. The acid then dissociates to form hydronium and bicarbonate ions, whereby bicarbonate ions displace surface hydroxides on the metal oxide interface, and hydronium ions result in protonation, effectively changing the surface potential. In agreement with this mechanism, control experiments were performed where only PEI polymer was used to functionalize SWNT-based devices. As expected, a minor response for the detection of CO₂ was observed, presumably as a result of direct protonation of the SWNT network. Further, because an aqueous hydration layer is responsible for the formation of carbonic acid, CO₂ exposure was performed under dry conditions. A SWNT device functionalized with Fe₂O₃ nanoparticles (1 mM) and PEI

(0.1 wt. %) was subjected to 5 min pulses of 5% CO₂ in 0% relative humidity; however, no response to CO₂ was observed. Further, sensitivity of the device to relative humidity was investigated as a control, revealing no observed response for 11-83% relative humidity created by varying saturated salt solutions.

As the proposed mechanism relies upon the formation of carbonic acid as a result of CO₂ interacting with a hydration layer, studies were performed by adding carbonic anhydrase, an enzyme that catalyzes the conversion of CO₂ to carbonic acid, to devices functionalized with Fe₂O₃ nanoparticles. Briefly, SWNT devices were first functionalized with Fe₂O₃ nanoparticles (1 mM in acetone) by drop-casting at a volume of 20 μL. Carbonic anhydrase (6 μM) was then drop-cast on the device at a volume of 5 μL and allowed to incubate in ambient. After approximately 20 min of incubation (solvation layer was still present), the device was placed in the PCB for testing and equilibrated in pure N₂ at 52% relative humidity as previously mentioned. CO₂ (1-10%) was cycled “on” and “off” at five minute increments, and corresponding changes in conductance were observed (Figure 7A). Similar to data presented previously, as CO₂ was cycled “on”, conductance was observed to decrease. One important note is that this device exhibited an overall greater change in conductance, which can be attributed to the efficient conversion of CO₂ to carbonic acid, a prominent characteristic of carbonic anhydrase. Moreover, while this device architecture allowed for increased sensitivity to CO₂, carbonic anhydrase quickly became inactivated after approximately three hours, possibly due to progressive dehydration, denaturation through joule heating,³⁷ or both.

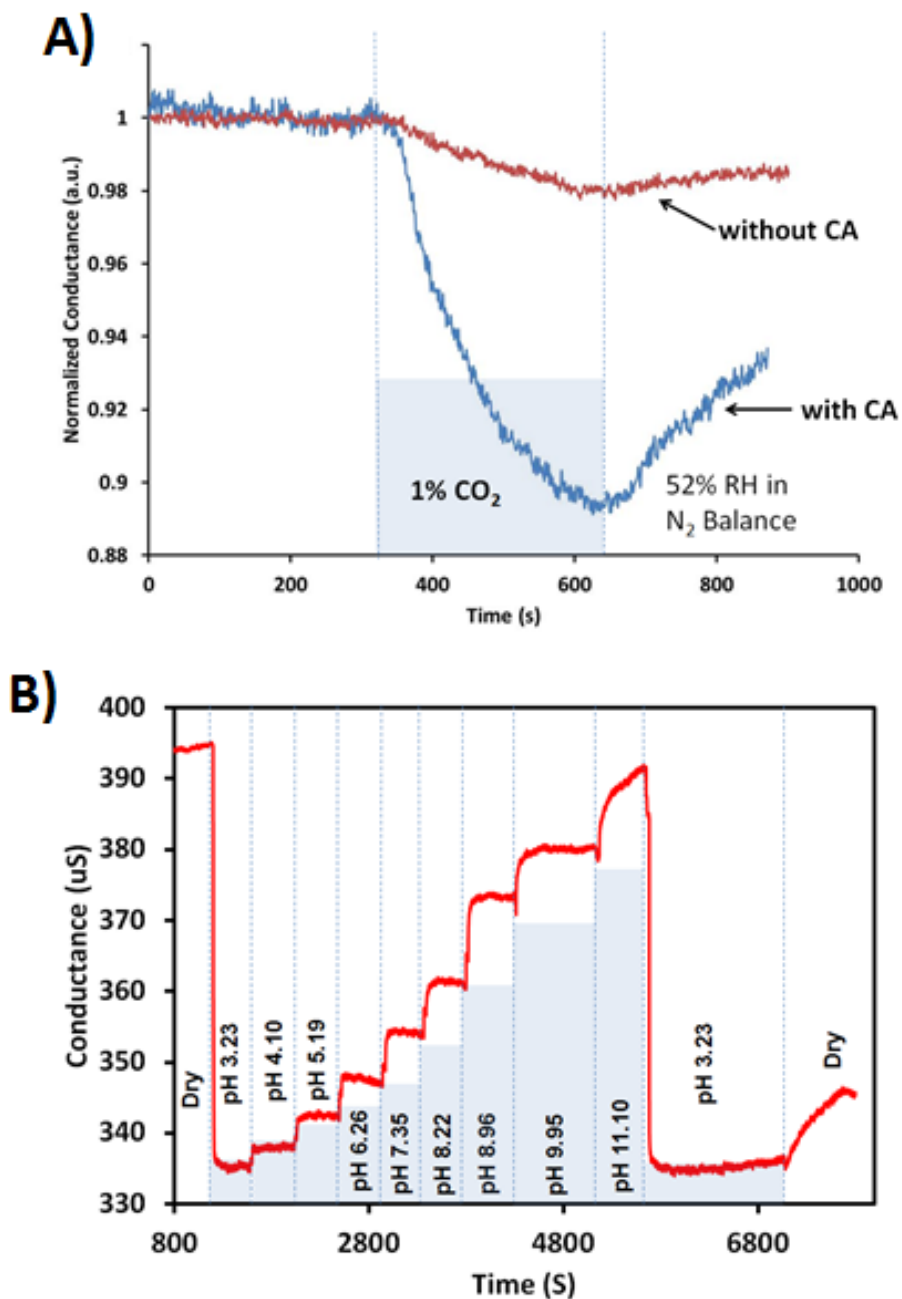


Figure 7 CO₂ detection mechanism experiments. A) Comparison of CO₂ gas response of devices functionalized with and without carbonic anhydrase (CA). B) Response SWNT/Fe₂O₃ NPs to varying pH buffered solutions.

To validate that observed responses were a result of an inherent change in pH, SWNT devices functionalized with Fe₂O₃ nanoparticles were used to examine solutions of varying pH. Note that no polymer layer was used as the pH solutions themselves will be acting as the hydration layer. Aqueous solutions buffered from pH values of 2 to 12 were prepared based on published methods.^{31, 32} Approximately 500 μL of the buffered solution was placed in a vial which was previously attached to the packaging containing the chip and then device characteristics, i.e. conductance measurements were recorded for some time. Subsequently, the solution was removed by suction from a micropipette and a new solution was added. It is important to note here that at no time did the micropipette tip come in contact with the surface of the device. A decrease in conductance (Figure 7B) is observed for decreasing concentrations of hydronium ions which agrees with the CO₂ gas measurements above, as CO₂ gas will decrease the pH of the hydration layer. However, one inherent weakness of such a pH sensitive system would be prone to cross-sensitivity to acidic gases. NO₂ sensitivity has been previously demonstrated utilizing a SWNT network device modified by PEI polymer.³⁸ Also, it is well known that NO₂ withdraws electronic density from SWNT-based devices.³⁹ However, the response of the PEI-coated devices was found to originate from protonation of the polymer layer. Nevertheless, it may be possible that the presence of metal oxide nanoparticles acting as localized electrostatic gates assist in the sensitivity of these devices. In this scenario, NO₂ would react with water to form an equilibrium reaction, where the final products are NO₂⁻, NO₃⁻, and H₃O⁺. The presence of other pH-altering gases such as SO₂ should then elicit a response as well.

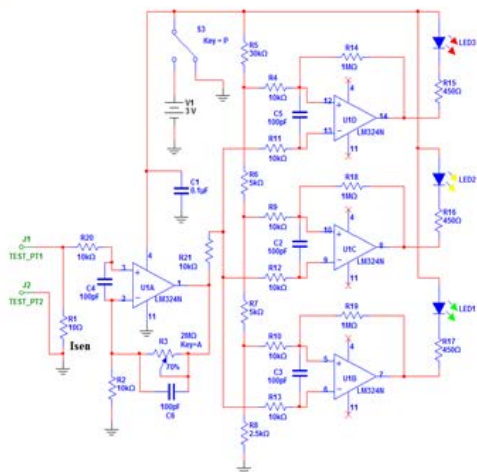
While reports of SWNT-based solid-state sensors have been reported previous for a variety of analytes including gases⁴⁰ and biological species¹⁸, it is important to note that the underlying mechanism may still be elusive as a result of multi-component systems. As

demonstrated here, the role of metal oxide nanoparticles is crucial for enhancing the sensitivity towards CO₂ gas. Further understanding of the surface functionalities influencing the P.Z.C. values of these metal oxide nanoparticles should thus allow for increased sensitivity in SWNT-based sensors.

2.1.3 Prototype Development

In order to test sensor chip integration, a battery powered handheld device has been developed through the University of Pittsburgh Chemistry Electronics Shop. The device uses the chip as a basic resistor and any change in the CO₂ levels will be observed by a change in light emitting diodes (LEDs) implanted on the device. Specifically, as the conductance of the device decreases upon exposure to breath, or any CO₂ source, there will be an observed decrease in the number of LEDs lit. Upon recovery all of the lights will relight. An adjustable resistor was implemented onto the prototype to account for any baseline drift. Future endeavors for the prototype involve integrating a USB or wireless hookup to be able to demonstrate both the crude LEDs along with more technical sensor data such as real time conductance measurements.

A)



Chemistry Electronics Shop



B)

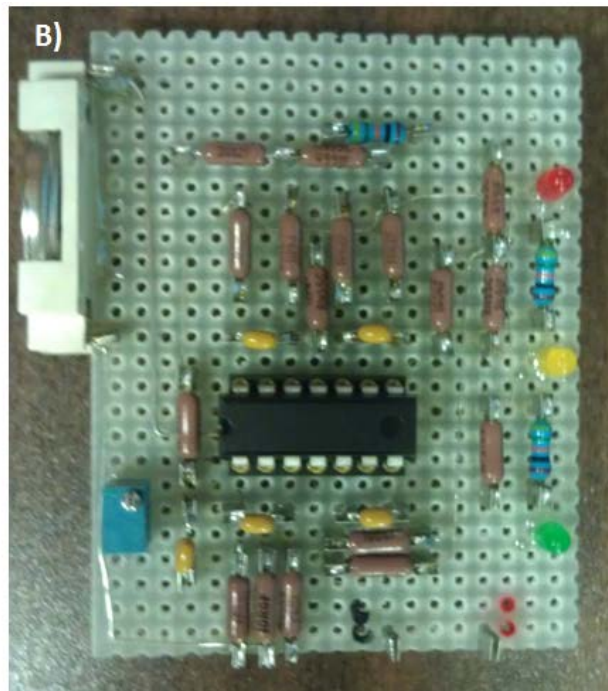


Figure 8 Prototype development. A) Electrical circuit diagram of a prototype device developed by the Pitt Chemistry Electronics shop based on technology of the CO₂ sensor device. B) Photograph of the device. The chip plugs into the black and red leads on the bottom right hand side of the photograph.

2.2 pH SENSING

Aqueous solutions receive a lot of attention as water covers over seventy percent of the planet and is vital for all known forms of life. In water, hydrogen atoms constantly transfer from one water molecule to another forming two charged species: the hydroxide ion (OH^-) and the hydronium ion (H_3O^+).⁴¹ While the relative concentrations of these two ions can vary, their product remains constant. Addition of foreign species, such as an acid or a base, can adjust the ratio of these two ions. The pH scale, a log concentration scale, has been developed to define such solutions, which is related to the concentration of hydronium ions by $\text{pH} = -\log [\text{H}_3\text{O}^+]$. Concurrently, the term pH originated from a French term meaning “power of hydrogen.” The pH of a solution can have a significant effect on chemical processes, therefore both the measurement and control of pH is important for materials, life, and environmental sciences. For example, it would be beneficial to monitor the pH inside the human body, however is very difficult with conventional technologies. Additionally, pH sensors which can be exposed to extraordinary conditions, such as extreme temperature and pressure, can be applied in geochemistry for monitoring pH levels to facilitate carbon sequestration technologies.

The most common pH sensors are glass electrodes with a salt solution-filled glass membrane limiting their applications. Some common problems associated with such electrodes include temperature dependence and errors in measurement in intense conditions (i.e., low pH and low ionic-strength solutions).⁴² Additionally, glass pH electrodes become sensitive to alkali-metal ions at high pH, degrade if dehydrated, and require calibration with a standard buffer, which has errors associated with itself. The field of ion-selective field-effect transistors (ISFETs) which started more than 40 years ago² has promised development of rugged, small, rapid response pH sensor devices. Additionally, ISFETs would not require hydration and would

be inert toward harsh environments. While there are numerous advantages of using ISFETs, one major limitation of the technology involves the requirement of a reference electrode ultimately limiting their size.⁴³ Continued efforts have been made to develop on-chip tiny reference electrodes; however because of these electrodes, ISFETs suffer the same limitations as conventional glass pH electrodes. Therefore a crucial factor for development of ISFET remains the reference electrode. We demonstrate here that carbon nanotube (CNT) based chemiresistors could alleviate the aforementioned problems. Specifically, a chemiresistor based on CNTs only requires measurement of the resistance of the nanotube network as a function of ion concentration, making measurement relatively easy.

To achieve the required specificity to hydronium ions (H_3O^+), carbon nanotubes were functionalized with conducting polymer. Recently, conducting polymers have been studied for detection of pH,⁴⁴⁻⁴⁶ as their electrical properties strongly depend on their protonation, and interestingly have shown very fast response when the sensing process occurs on the surface of the polymer.⁴⁷ However, a major problem of all organic conductors is their limited chemical stability. CNTs can help to stabilize polymers, increasing the lifetime of the sensor device,⁴⁸ while additionally increasing the aspect ratio of the polymer for facile integration into micrometer sized electronics. It is apparent that by combining the two types of materials, synergetic effects are observed: First, the polymer contributes to the device selectivity, while the carbon nanotubes provide a sensitive and robust platform necessary to chemically stabilize the polymer. Polypyrrole (PPy) and polyaniline (PAni) polymers have been combined with nanotubes toward the development of solid state pH sensor devices using only two terminal conductance measurements.⁴⁹

We have developed a pH sensitive device by combining oxidized SWNTs (o-SWNTs) with a conducting polymer, poly(1-aminoanthracene) (PAA). The pH levels can be monitored electrically by configuring the nanotube/polymer composite as a chemiresistor. Specifically, the conductance of the PAA/o-SWNT network scales linearly with respect to changes in the pH of the solution.

2.2.1 Experimental Details

Materials: Pristine single-walled carbon nanotubes (SWNTs) were purchased from Carbon Solutions, Inc (P2). 1-aminoanthracene (AA), anhydrous acetonitrile (MeCN) and $\text{FeSO}_4 \cdot 7 \text{H}_2\text{O}$ powder and were obtained from Sigma Aldrich. Tetrabutylammonium perchlorate (TBAP) was prepared from the reaction of tetraalkylammonium bromide (Sigma Aldrich) and HClO_4 . The reaction product was recrystallized four times and dried under vacuum at room temperature overnight. Aqueous solutions buffered from pH values of 2 to 12 were prepared based on published methods.^{31,32} The pH of the buffered solution was measured using a Mettler Toledo SevenGo SG2 pH meter. The pH meter was calibrated with standard buffered solutions obtained from J. T. Baker.

Preparation of conductive carboxylated SWNTs: SWNTs were dispersed in 20 mL of concentrated $\text{H}_2\text{SO}_4/\text{HNO}_3$ (3:1). The mixture was subsequently sonicated for 2 hrs at 40 °C in an ultrasonic bath (5510 Brasonic) to yield oxidized SWNTs (o-SWNTs) with lengths around 300 nm. Carboxylic acid groups were confirmed through FT-IR spectroscopy. FT-IR spectra were recorded as thin film as KBr pellets on an Avatar 380 Nicolet FI-IR spectrometer. Upon

completion, the mixture was added drop wise to 100 mL of cold distilled water and then filtered through 0.2- μm pore size PTFE (Teflon) laminated filter paper and then washed with water until no residual acid was present.

Sensor Device Fabrication: Silicon chips with 300 nm thermal oxide layer and pre-fabricated interdigitated Au electrodes (MEMS and Nanotechnology Exchange) were wire-bonded into a 40-pin CERDIP package, followed by passivation of the system with PDMS. Aqueous suspensions (0.3 μL) of o-SWNTs in N,N-dimethylformamide (DMF) were dropcast onto the Si chips and allowed to dry in ambient. PAA was subsequently added to the o-SWNT network *via* electropolymerization (EP) of the monomeric units, AA, into the polymer, PAA.⁵⁰ EP was performed with a using a CH Instruments electrochemical analyzer with o-SWNTs configured as the working electrode in a standard three-electrode single compartment electrochemical cell. A platinum wire and a Ag/AgCl quasi-reference electrode were used as the auxiliary and reference electrodes, respectively. Anhydrous acetonitrile was used as the electrolyte solution which contained the supporting electrolyte, TBAP (0.1 M), and the monomeric units, AA (1 mM). PAA was prepared on the o-SWNT film using cyclic voltammetry by sweeping the electrode potential between 0 and + 0.8 V at rate of 0.05 V/s. 24 hr prior to testing, the electrodes were conditioned in an aqueous solution containing a phosphate buffer (pH = 5.60). The formation as well as morphology of PAA was characterized through SEM on a Philips SL30 FEG microscope at an accelerating voltage of 10 keV.

Electrical Measurement: For pH-solution sensing, conductance of the nanotube network was measured for a constant voltage (V_{SD}) of 50 mV with a Keithley 2400 source meter for

varying pH buffered solutions. The chip was exposed to 500 μ L of the buffered solution via deposition by a micropipette. Specifically, the conductance through the nanotube network was determined by measuring the current at a constant bias voltage of 50 mV.

2.2.2 Results and Discussion

Configuring the device as a chemiresistor allows for direct real-time electrical measurements of the system as a function of analyte as well as analyte concentration. A chemiresistor is a device that changes resistance upon exposure to an analyte of interest. The PAA/o-SWNT can easily be integrated on top of a Si/SiO₂ chip containing interdigitated gold electrode. First, o-SWNTs in DMF are dropcast onto the chip and dried in ambient, followed by formation of PAA *via* electropolymerization (EP). Figure 9A depicts a typical device setup for EP of aminoanthracene (AA) to poly(1-aminoanthracene) (PAA).⁵⁰ In this three electrode electrochemical cell, a network of oxidized single-walled carbon nanotubes (o-SWNTs) is used as the working electrode (W.E.). The potential of the W.E. is varied with respect to a quasi-reference electrode (R.E.) (Ag/AgCl), while the Pt wire auxiliary electrode (A.E.) is used to monitor the current produced without changing the potential of the R.E. By sweeping the potential of the working electrode while the system is submerged into an electrolyte solution (TBAP in MeCN) containing AA monomeric units, PAA is formed. More specifically by sweeping the potential between 0 to + 0.8V at a sweep rate of 0.05 V/s, one cyclic voltammetry (CV) cycle is completed, and thus formation of PAA. The resulting current, plotted *versus* potential in Figure 9C, tells us information about the EP process. With an increase in the number of cycles from 1 (red) to 30 cycles (purple), peaks for the oxidation of the monomeric unit (A1) disappear and a peak for dimer and oligomer units (A2) appears. The formation of PAA has also

been confirmed by SEM. An image of an EP prepared device after 50 CV cycles is given in Figure 9B showing the morphology of the polymer. A higher magnification image reveals o-SWNTs that are not connected to the nanotube network. Since these o-SWNTs were not connected to the “W.E.” no polymer was deposited onto them.

By holding the voltage passing through the o-SWNT network (V_{SD}) constant and measuring the resulting current (I_{SD}) as a function of analyte, sensitivity of the chemiresistor to various analytes can be determined with relative ease. An inert plastic vial was attached to the packaging of the chip in order to hold the varying pH solutions. Figure 10A presents a conductance *versus* time plot for a PAA/o-SWNT device (V_{SD}) showing response to buffered solutions from pH = 3 to pH = 11. An increase in conductance is observed for increasing amounts of H_3O^+ ion (Brønsted-Lowry acid). Specifically increasing the amount of H_3O^+ ions in solution withdraws electrons from the partially filled SWNT VB increasing the electrical conductivity. Furthermore, plotting the response of the device *versus* pH (Figure 10B) reveals a linear calibration curve with very little variance ($R^2 > 0.99$). This scaling relationship between response and pH is necessary toward development of a sensor device, and the deviation between the responses is minuscule (error bars are very small). The PAA coated o-SWNT electrodes were robust as even 8 days after fabrication and initial testing, the device characteristics have not severely degraded.

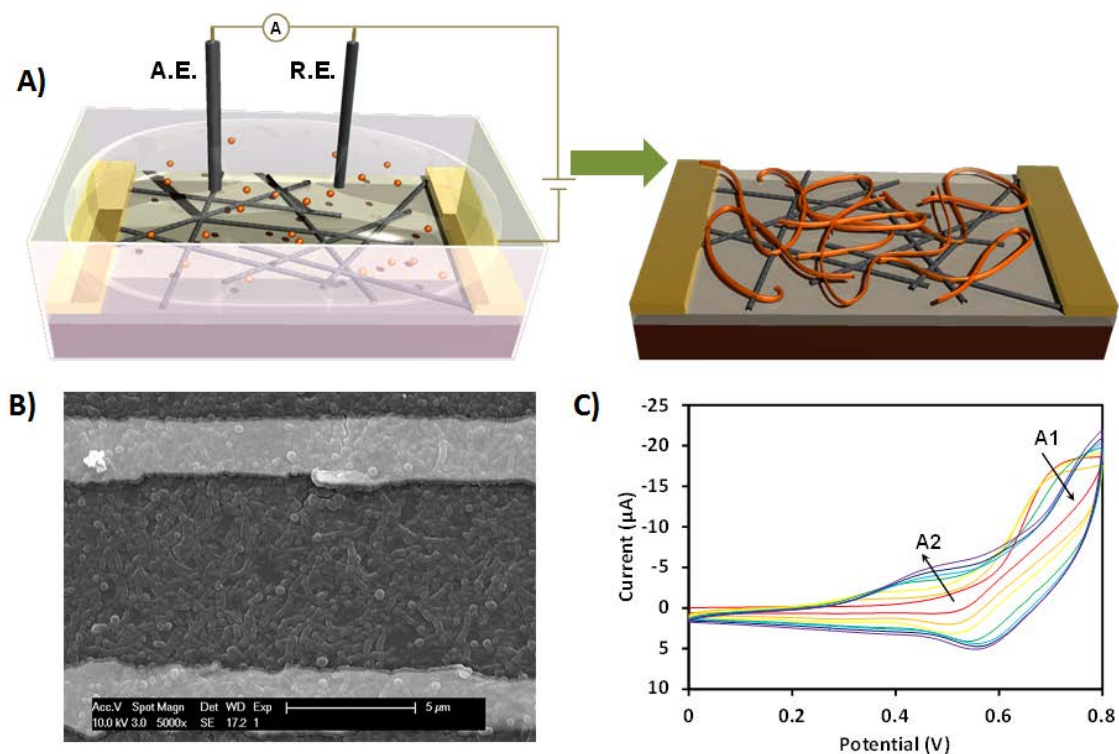


Figure 9 pH sensor material characterization. A) Generalized schematic of electropolymerization (EP) of poly(1-aminoanthracene) (PAA) onto oxidized single-walled carbon nanotubes (o-SWNTs) using the nanotube network as the working electrode (W.E.) accompanied by a Ag/AgCl quasi reference electrode (R.E.) and a Pt wire auxiliary electrode (A.E.). The whole system was submersed into an electrolyte solution (TBAP in MeCN) containing the aminoanthracene (AA) monomeric units (represented by the orange spheres). Performing cyclic voltammetry (CV) results in formation of PAA, and after removal of the liquid cell, the device is ready for testing. B) Microscopy images of a typical devices (after 50 CV cycles). Scanning electron microscopy (SEM) images depict the morphology of the polymer formed. C) Cyclic voltammetry of EP of PAA onto o-SWNT. As the number of cycles increase, from 1 (red) to 30 cycles (purple), the oxidation peaks for the AA monomeric unit (A1) disappear and the peak for PAA (A2) appear.

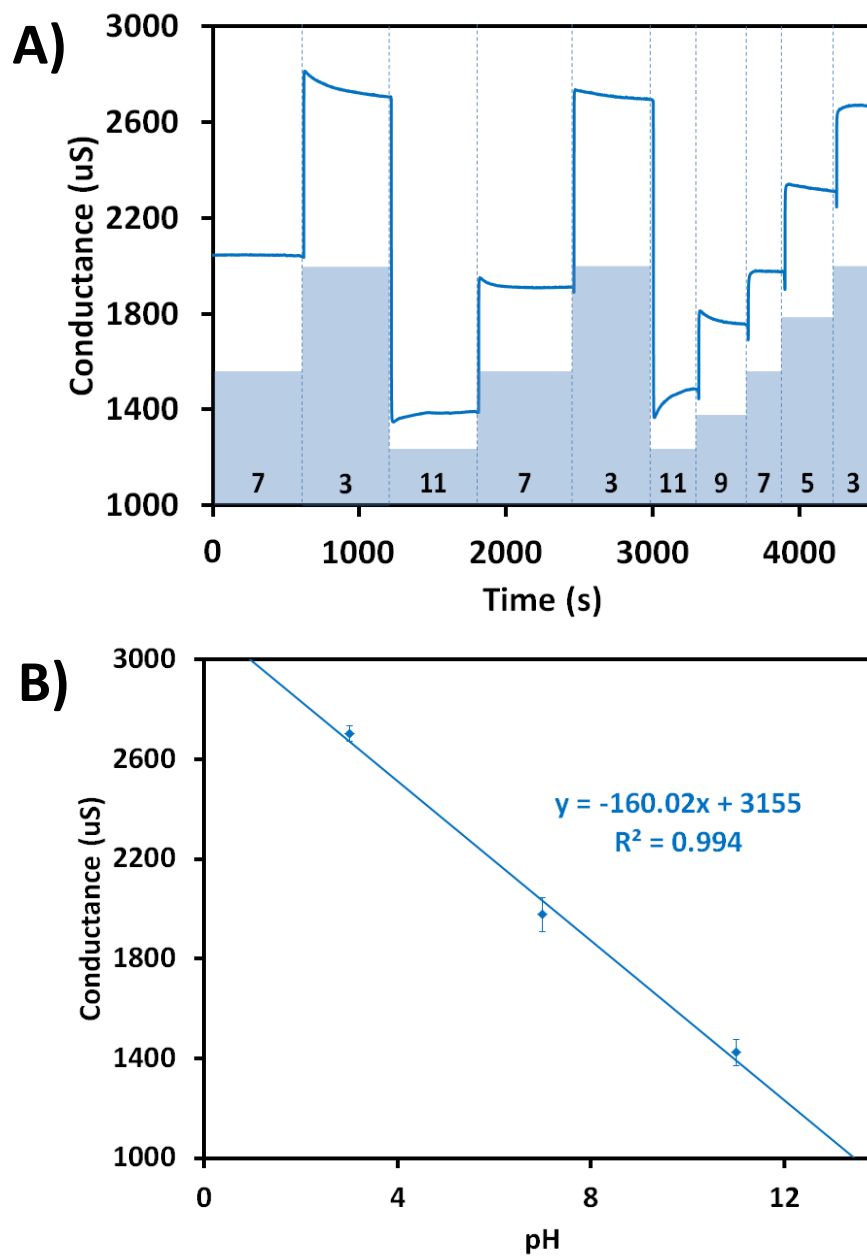


Figure 10 Electrical measurements of PAA/o-SWNT. A) Conductance vs. time for PAA/o-SWNT (20 cycles) for pH from 11 to 3. An increase in conductance is observed for increasing amounts of hydronium ions in solution. B) Three-point calibration curve (conductance vs. concentration) of the device in A with error bars depicting the first standard deviation.

Field-effect transistor measurements were investigated in order to elucidate the mechanism in which the o-SWNT/PAA composite responds to changes in pH. By holding the voltage through the nanotube network constant (50 mV) and sweeping the gate voltage, we can understand the semiconducting properties of the composite. Figure 11A depicts the transfer characteristic curve of the composite in a various pH buffered solution, which reveals that the conductivity of the composite “turns off” at positive gate voltage. This is indicative of a p-type semiconductor. As the pH decreases, observation of the FET characteristics reveals a decrease in the conductance at a negative gate voltage. This is opposite to the trend observed for the conductance vs. time measurements previously presented. One important note: all conductance vs. time measurements were performed with a “floating gate.” When conductance vs. time measurements were investigate with a fixed gate of -0.2 V, conductance decreased for decreasing pH (Figure 11B), agreeing with the FET characteristics.

The pH response of PAA coated o-SWNTs is primarily related to the conductivity of PAA. Due to the similarities of PAA and PANi, looking at the mechanism of pH detection of PANi can shed insight into the detection mechanism for PAA. PANi’s pH sensitivity is attributed to the reversible acid/base doping of the polymer which exhibits a measurable effect on the electrical properties of the polymer.⁵¹ Specifically, acid doping of PANi consists of the addition of a proton and a counter ion for every imine nitrogen in the polymer backbone, causing a significant increase in the conductivity of PANi. This is in agreement with the electrical results obtained from PAA in this report.

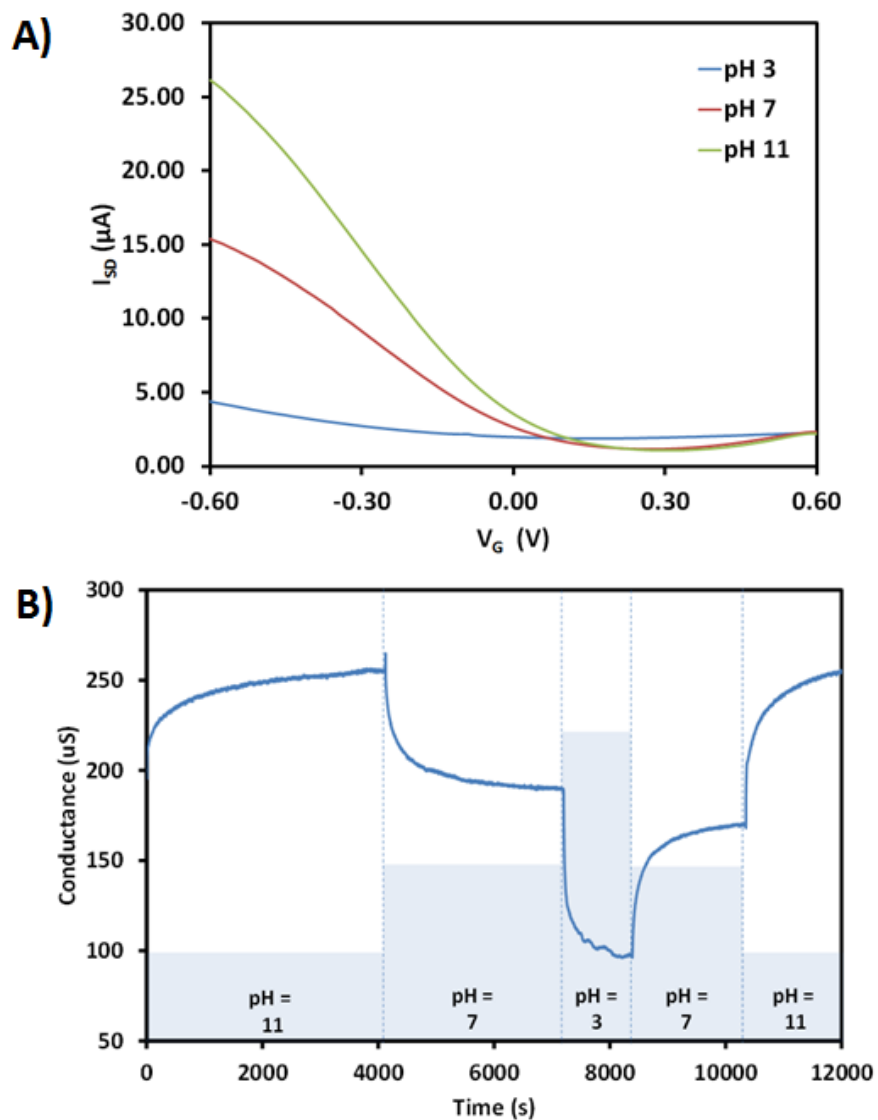


Figure 11 Field-effect transistor characterization of PAA/o-SWNT. A) Field-effect transistor characteristics of o-SWNT/PAA for varying pH buffered solutions. B) Conductance vs. time measurements at a fixed gate of -0.2 V.

Based on knowledge gained from the CO₂ sensor device, this pH sensor was tested for CO₂ gas sensitivity. Preliminary studies suggest that passing CO₂ over the PAA coated o-SWNT was not enough to elicit a response. However, after functionalizing the device with a hydration source, specifically a drop of sodium bicarbonate, the device responded to CO₂ gas. An increase in conductance (seen in Figure 12A) agrees with a decrease in pH of this sensor, which is known to occur upon CO₂ gas exposure to a hydration source. More work still needs to be done to develop a sensor that scales with the concentration of CO₂ gas.

Additionally, this device has been further functionalized with Pd NPs and preliminary results reveal H₂ gas sensitivity. The device has responded to concentrations of H₂ gas as low as 16 ppm (Figure 12B). It has been previously shown that a pH sensitive polymer has been applied to detection of H₂ gas using Pd metal NPs.⁵² Upon introduction of H₂ gas to Pd NPs the gas becomes very unstable and dissociates into hydrogen atoms. The protons are assumed to be causing the change in concentration of the o-SWNT network. Future endeavors involve characterizing the material, optimizing the concentration of Pd NPs and fully characterizing the sensor.

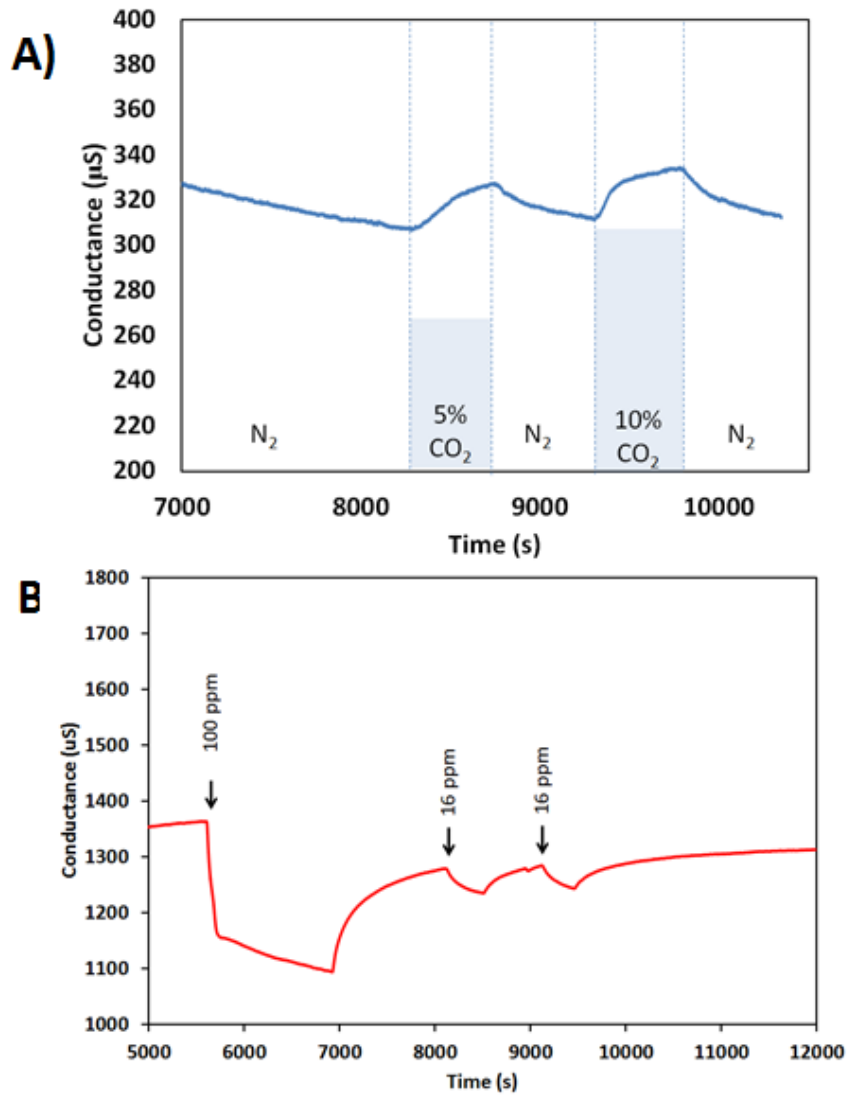


Figure 12 Further functionalization of PAA/o-SWNT for detection of other analytes. Further functionalization of the SWNT/PAA composite allows for sensitivities toward A) CO₂ gas and B) H₂ gas. These gases will not elicit a change in response without their respective functionalizations.

Future studies for the pH sensor entail optimizing the sensor to detect pH in relevant ranges in order to apply the sensor for real time monitoring of pH. Measurements of blood could be applied to wound care and blood analysis, while monitoring of pools and fish tanks could offer personal uses for such a sensor. In order to optimize the pH sensor previously described for such an application, numerous parameters can be adjusted. First the amount and way in which the polymer is deposited can be changed. Simply by varying the number of cyclic voltammetric sweeps, adjustment of the amount of the polymer deposited on the SWNT network can be performed which may allow for optimization of the device. Additionally other polymerization techniques, such as deposition at a constant potential could help to sensitize the device. In addition to fully optimizing the device parameters, cross sensitivity of the device needs to be determined for varying analytes in questions. In addition to other cations such as sodium and potassium, complex components of blood, such as human serum albumin and DNA need to be investigated for cross sensitivity.

3.0 FUTURE ENDEAVORS (TOWARDS BIOSENSING)

SWNTs have shown great promise toward applications in biosensing. For example, groups have shown that functionalized SWNTs have exhibited enhanced sensitivity toward DNA,⁵³⁻⁵⁵ proteins,⁵⁶⁻⁵⁹ and enzymes.⁶⁰ We will use the mechanistic insight gained from studying the interactions of SWNTs with pH and salt to develop methods for investigating new biosensors based on SWNTs. Typically a binding assay for such biosensors includes a receptor, bound to the SWNT, and a target analyte. The receptor, such as a nucleotide, aptamer, antibody or cofactor, acts as a recognition site for the complementary biomolecule. Specifically, I would like to apply such systems toward the detection of diseases such as Chronic Traumatic Encephalopathy (CTE). CTE results in high levels of phosphorylated tau proteins which causes neurofibrillary tangles. The current method of detection requires sampling of spinal fluid due to the high detection limit of the ELISA sensor. By taking advantage of the ultrasensitivity of SWNT, a biosensor capable of detecting the phosphorylated tau proteins in blood may be developed. Receptors, the antibodies to the protein antigen in this case, will be attached to the sidewall of SWNT and upon introduction of serum, conductivity changes will occur only if the phosphorylated tau proteins are present. The design of such a biosensor could also be applied to detect other biologically relevant molecules such as cancer markers.

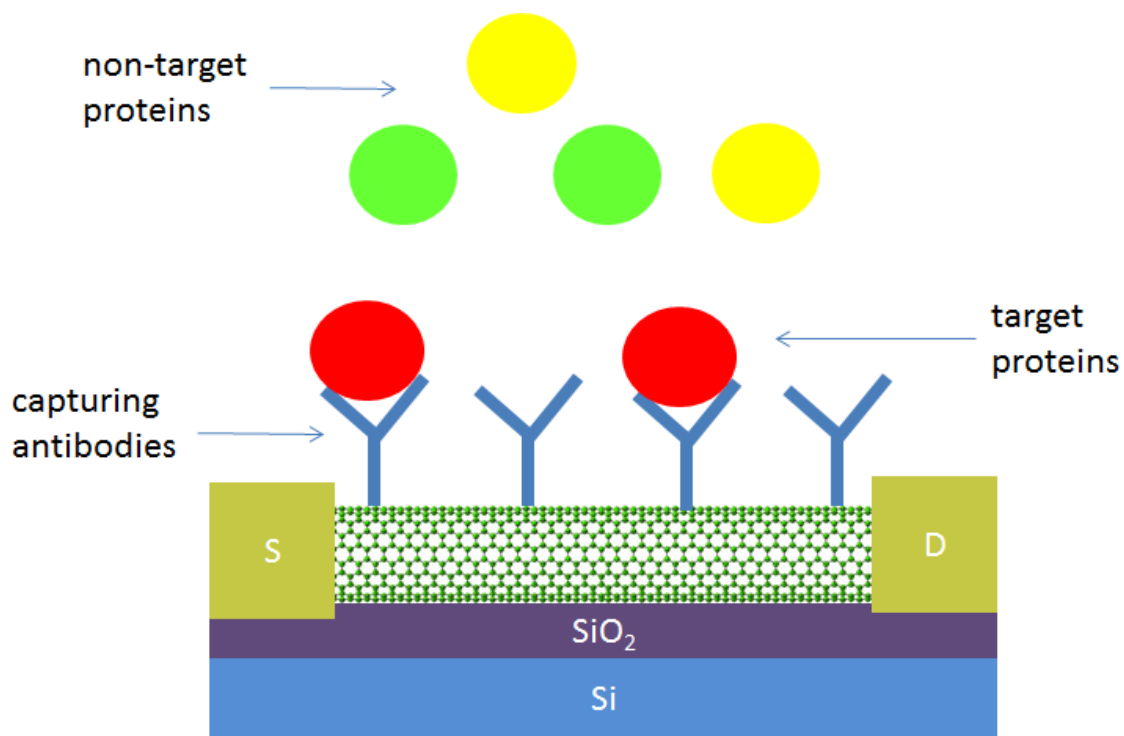


Figure 13 Proposed scheme for biosensor development. SWNT functionalized with specific antibodies will capture complementary antigens causing changes in the conductivity of the SWNT network. Non target antigens will not bind to the receptor and therefore would not change the electrical properties of the SWNT network.

BIBLIOGRAPHY

1. Kroto, H. W.; Heath, J. R.; O'Brien, S. C.; Curl, R. F.; Smalley, R. E. *Nature* **1985**, 318, 162-163.
2. Radushkevich, L. V.; Iukyanovich, V. M. *Zurn Fisic Chim* **1952**, 26, 88-95.
3. Iijima, S. *Nature* **1991**, 354, (6348), 56-58.
4. Odom, T. W.; Huang, J.-L.; Kim, P.; Lieber, C. M. *J. Phys. Chem. B* **2000**, 104, (13), 2794-2809.
5. Balasubramanian, K.; Burghard, M. *Small* **2005**, 1, (2), 180-192.
6. Anantram, M. P.; Léonard, F. *Rep. Prog. Phys.* **2006**, 69, (3), 507.
7. Kataura, H.; Kumazawa, Y.; Maniwa, Y.; Umezumi, I.; Suzuki, S.; Ohtsuka, Y.; Achiba, Y. *Synth. Met.* **1999**, 103, (1-3), 2555-2558.
8. Zangwill, A., *Physics at Surfaces*. Cambridge University Press: Cambridge, New York, 1988.
9. Javey, A.; Guo, J.; Wang, Q.; Lundstrom, M.; Dai, H. *Nature* **2003**, 424, (6949), 654-657.
10. Suzuki, S. *Appl. Phys. Lett.* **2000**, 76, (26), 4007.
11. Zhao, J.; Han, J.; Lu, J. P. *PhRvB* **2002**, 65, (19), 193401.
12. Shiraishi, M.; Ata, M. *Carbon* **2001**, 39, (12), 1913-1917.
13. Kuzmich, O.; Allen, B. L.; Star, A. *Nanotechnology* **2007**, 18, (37), 375502.
14. Tans, S. J.; Verschueren, A. R. M.; Dekker, C. *Nature* **1998**, 393, (6680), 49-52.
15. Martel, R.; Schmidt, T.; Shea, H. R.; Hertel, T.; Avouris, P. *Appl. Phys. Lett.* **1998**, 73, (17), 2447-2449.
16. Chen, Z.; Appenzeller, J.; Knoch, J.; Lin, Y.-m.; Avouris, P. *Nano Letters* **2005**, 5, (7), 1497-1502.

17. Appenzeller, J.; Knoch, J.; Derycke, V.; Martel, R.; Wind, S.; Avouris, P. *Phys. Rev. Lett.* **2002**, 89, (12), 126801.
18. Allen, B. L.; Kichambare, P. D.; Star, A. *Adv. Mater.* **2007**, 19, (11), 1439-1451.
19. Levine, R. L.; Wayne, M. A.; Miller, C. C. *New Engl. J. Med.* **1997**, 337, (5), 301-306.
20. White, C. M.; Smith, D. H.; Jones, K. L.; Goodman, A. L.; Jikich, S. A.; LaCount, R. B.; DuBose, S. B.; Ozdemir, E.; Morsi, B. I.; Schroeder, K. T. *Energy & Fuels* **2005**, 19, (3), 659-724.
21. Lindroth, R. L.; Kopper, B. J.; Parsons, W. F. J.; Bockheim, J. G.; Karnosky, D. F.; Hendrey, G. R.; Pregitzer, K. S.; Isebrands, J. G.; Sober, J. *Environ. Pollut.* **2001**, 115, (3), 395-404.
22. Folke, M.; Cernerud, L.; Ekström, M.; Hök, B. *Medical and Biological Engineering and Computing* **2003**, 41, (4), 377-383.
23. Yao, S.; Hosohara, S.; Shimizu, Y.; Miura, N.; Futata, H.; Yamazoe, N. *Chem. Lett.* **1991**, 20, (11), 2069-2072.
24. Haeusler, A.; Meyer, J.-U. *Sensors Actuators B: Chem.* **1996**, 34, (1-3), 388-395.
25. Marazuela, M. D.; Moreno Bondi, M. C.; Orellana, G. *Sensors Actuators B: Chem.* **1995**, 29, (1-3), 126-131.
26. Cadle, S. H.; Groblicki, P. J.; Stroup, D. P. *Anal. Chem.* **1980**, 52, (13), 2201-2206.
27. Sivaramakrishnan, S.; Rajamani, R.; Smith, C. S.; McGee, K. A.; Mann, K. R.; Yamashita, N. *Sensors Actuators B: Chem.* **2008**, 132, (1), 296-304.
28. Fasching, R.; Keplinger, F.; Hanreich, G.; Jobst, G.; Urban, G.; Kohl, F.; Chabicovsky, R. *Sensors Actuators B: Chem.* **2001**, 78, (1-3), 291-297.
29. Varghese, O. K.; Kichambre, P. D.; Gong, D.; Ong, K. G.; Dickey, E. C.; Grimes, C. A. *Sensors Actuators B: Chem.* **2001**, 81, (1), 32-41.
30. Star, A.; Han, T. R.; Joshi, V.; Gabriel, J. C.; Grüner, G. *Adv. Mater.* **2004**, 16, (22), 2049-2052.
31. Robinson, R. A., *Electrolyte solutions; the measurement and interpretation of conductance, chemical potential, and diffusion in solutions of simple electrolytes*. Butterworths: London, 1965.
32. McIlvaine, T. C. *J. Biol. Chem.* **1921**, 49, (1), 183-186.
33. <http://sourceforge.net/projects/zephyr>
34. Rockland, L. B. *Anal. Chem.* **1960**, 32, (10), 1375-1376.

35. Kosmulski, M., *Chemical Properties of Material Surfaces*. Marcel Dekker, Inc.: New York, NY, USA, 2001.
36. Baltrusaitis, J.; Grassian, V. H. *J. Phys. Chem. B* **2005**, 109, (25), 12227-12230.
37. Arata, H. F.; Rondelez, Y.; Noji, H.; Fujita, H. *Anal. Chem.* **2005**, 77, (15), 4810-4814.
38. Oleksandr, K.; et al. *Nanotechnology* **2007**, 18, (37), 375502.
39. Kong, J.; Franklin, N. R.; Zhou, C.; Chapline, M. G.; Peng, S.; Cho, K.; Dai, H. *Science* **2000**, 287, (5453), 622-625.
40. Kauffman, D. R.; Star, A. *Angew. Chem. Int. Ed.* **2008**, 47, (35), 6550-6570.
41. Tro, N. J., *Principles of Chemistry: A Molecular Approach*. Pearson Education, Inc: Upper Saddle Ridge, New Jersey, 2010.
42. Skoog, D. A.; Holler, F. J.; Crouch, S. R., *Principles of Instrumental Analysis*. Sixth Edition ed.; Thomson Brooks/Cole: Belmont, CA, 2007.
43. Bergveld, P. *Sensors Actuators B: Chem.* **2003**, 88, (1), 1-20.
44. Talaie, A. *Polymer* **1997**, 38, (5), 1145-1150.
45. Kaden, H.; Jahn, H.; Berthold, M. *Solid State Ionics* **2004**, 169, (1-4), 129-133.
46. Gao, W.; Song, J. *Electroanalysis* **2009**, 21, (8), 973-978.
47. Jin, G.; Novish, J.; Too, C.; Wallace, G. *CAP* **2004**, 4, 366.
48. Ding, M.; Tang, Y.; Gou, P.; Reber, M. J.; Star, A. *Adv. Mater.* **2011**, 23, (4), 536-540.
49. Liao, Y.; Zhang, C.; Zhang, Y.; Strong, V.; Tang, J.; Li, X.-G.; Kalantar-Zadeh, K.; Hoek, E. M. V.; Wang, K. L.; Kaner, R. B. *Nano Letters* **2011**, 11, (3), 954-959.
50. Faria, R. C.; Bulhões, L. O. S. *Electrochim. Acta* **1999**, 44, (10), 1597-1605.
51. Virji, S.; Huang, J.; Kaner, R. B.; Weiller, B. H. *Nano Letters* **2004**, 4, (3), 491-496.
52. Hoki, T.; Takahashi, H.; Suzuki, S.; Mizuguchi, J. *Sensors Journal, IEEE* **2007**, 7, (5), 808-813.
53. Star, A.; Tu, E.; Niemann, J.; Gabriel, J.-C. P.; Joiner, C. S.; Valcke, C. *Proc. Natl. Acad. Sci. USA* **2006**, 103, (4), 921-926.
54. Gui, E.-L.; Li, L.-J.; Lee, P. S.; Lohani, A.; Mhaisalkar, S. G.; Cao, Q.; Kang, S. J.; Rogers, J. A.; Tansil, N. C.; Gao, Z. *Appl. Phys. Lett.* **2006**, 89, (23), 232104-3.

55. Dong, X.; Lau, C. M.; Lohani, A.; Mhaisalkar, S. G.; Kasim, J.; Shen, Z.; Ho, X.; Rogers, J. A.; Li, L. J. *Adv. Mater.* **2008**, 20, (12), 2389-2393.
56. Star, A.; Gabriel, J.-C. P.; Bradley, K.; Grüner, G. *Nano Letters* **2003**, 3, (4), 459-463.
57. So, H.-M.; Won, K.; Kim, Y. H.; Kim, B.-K.; Ryu, B. H.; Na, P. S.; Kim, H.; Lee, J.-O. *J. Am. Chem. Soc.* **2005**, 127, (34), 11906-11907.
58. Maehashi, K.; Katsura, T.; Kerman, K.; Takamura, Y.; Matsumoto, K.; Tamiya, E. *Anal. Chem.* **2006**, 79, (2), 782-787.
59. Vedala, H.; Chen, Y.; Cecioni, S.; Imberty, A.; Vidal, S. b.; Star, A. *Nano Letters* **2011**, 11, (1), 70-175.
60. Besteman, K.; Lee, J.-O.; Wiertz, F. G. M.; Heering, H. A.; Dekker, C. *Nano Letters* **2003**, 3, (6), 727-730.